Int. J. Heat Mass Transfer. Vol. 28, No. 9, pp. 1657–1667, 1985
Printed in Great Britain

0017-9310/85 $3.00 + 0.00

A high sensitivity, fast response heat flux sensor

A. R. P. VAN HEININGEN, W. J. M. DOUGLAS and A. S. MUJUMDAR
Pulp and Paper Research Institute of Canada, and Department of Chemical Engineering, McGill University, Montreal, Quebec, Canada H3A 2A7

(*Received* 5 *June* 1984 *and in final form* 5 *February* 1985)

Abstract—A high sensitivity, fast response heat flux sensor was developed for heat flux measurement at a moving surface subjected to rapidly fluctuating heat flux. The sensor is a gold thin film resistance thermometer on a non-conducting substrate. Mounted flush with the moving surface, the sensor measures instantaneous surface temperature with a resolution of about 0.002°C at sampling speeds up to 5000 s^{-1}. Local heat flux is obtained through solution of the unsteady heat conduction equation. Heat transfer profiles are generated with this technique for the case of plane jets impinging on surfaces moving at speeds up to 12 m s^{-1}.

INTRODUCTION

EXPERIMENTAL studies of heat transfer involving moving surfaces, unsteady flows or rapidly moving heat sources often require a heat flux sensor for accurate measurement of the (nearly) instantaneous local heat transfer variation. The measurement technique presented here was developed in connection with an experimental program designed to determine the local heat transfer distribution under a heated plane turbulent air jet impinging on a rotating permeable cylinder. The latter study is part of a broader research program motivated by the development of a combined impingement and through drying process (called the "Papridryer") for drying of newsprint [1, 2]. The technique, however, is generally applicable for measurement of heat transfer to or from moving surfaces.

The critical feature and most challenging aspect of the present impinging jet study is the method for measuring local heat transfer at a point on the impingement surface which has a transient time under the nozzle in the order of 1 ms. As a consequence of the high rotational speeds, the maximal surface temperature variation over a complete revolution is only of the order of 0.1°C [3]. The requirement of measuring local heat transfer under such conditions could only be met by mounting a high sensitivity, fast response heat flux sensor flush with the impingement surface and by using a computer for on-line data acquisition and data processing.

SELECTION OF THE HEAT FLUX SENSOR

Fast response heat flux gauges have been used for applications such as determination of cylinder wall temperature variations in reciprocating engines and determination of heat flux rates to aerodynamic models, in shock tubes and shock tunnels [4]. The two basic techniques used are thin-film surface thermometry and thick-film calorimetry. Another instrument, the hot film probe, which is normally used for skin friction measurements, was first considered for heat transfer measurements in this work as its use had been reported in previous studies [5, 6]. However, as our analysis established that such use was invalid because of the inapplicability of the analogy between heat and momentum transfer [7], this technique was rejected. Selection of the heat flux sensor for the present work was aided by the excellent study of Baines [8] on unsteady heat flux sensors, which also included the gradient sensor and thin disk or Gardon foil. For short measuring times or rapidly fluctuating heat flux, the thin- and thick-film probes are preferred. As the thin-film sensor is the more sensitive gauge, it was selected for the present investigation. A thin-film sensor is essentially a slab, the surface temperature of which is measured. The thickness of the slab must be such that it may be considered thermally 'semi-infinite' over the time period of interest.

Because the cyclic variation in surface temperature was in the present case very small, a resistance thermometer rather than a thermocouple (or thermopile) was chosen for measurement of the thin-film temperature. It can be shown [3] that the sensitivity S_s of a thin-film resistor at the maximum allowable self-heating power q_{sm} is

$$S_s = \alpha_s L(\delta q_{sm}/d)^{1/2}. \quad (1)$$

The highest sensitivity is obtained for a stable conductor having a maximum value of $\alpha_s\delta^{1/2}$; α_s and δ being the thermal coefficient of resistance and resistivity of the film, respectively. The 'bulk' values of $\alpha_s\delta^{1/2}$ for nickel, platinum and gold are 0.0181, 0.0128 and 0.0061 $(\mu\Omega\ \text{cm})^{1/2}\ K^{-1}$, respectively. Thus of these three alternative materials, nickel provides the most sensitive and gold the least sensitive thin-film resistance thermometer, assuming that the thin-film values of α_s and δ vary proportional to the 'bulk' values. However, a nickel film was found to be unstable in moist air while platinum was very difficult to deposit because of the high vaporization temperature required. As gold films were stable in moist air, acetone and benzene, adhered

NOMENCLATURE

a_s	thermal diffusivity of pyroceram sensor [$m^2 s^{-1}$]
c_p	specific heat [$J kg^{-1} K^{-1}$]
d	thickness of gold film [m]
h	layer thickness in calculation procedure of heat flux in equation (6) [m]
H	spacing, nozzle-to-impingement surface [mm]
L	effective length of gold film [m]
M_{V_s}	impingement surface velocity mass ratio, $\rho_s V_s/(\rho_j U_j)$
N_R	number of rotations
Nu	Nusselt number, $\alpha w/\lambda$
Nu_{jm}	Nusselt number at the secondary heat transfer peak
Δp	pressure difference over jet nozzle [mm H_2O]
q	heat flux [$W m^{-2}$]
q_{sm}	maximum self-heating power of sensor in equation (1) [$W m^{-2}$]
R_s	resistance of sensor [Ω]
R_v	resistance of variable resistor in Wheatstone bridge sensor circuit [Ω]
Re	Reynolds number, $\rho U w/\mu$
S_s	sensor sensitivity [$V K^{-1}$]
S_b	sensitivity of heat flux sensor system [$V K^{-1}$]
t	time [s]
T	temperature [°C]
$T_{r,t}$	temperature in equation (5) [°C]
U_j	jet velocity at nozzle exit [$m s^{-1}$]
v	voltage across the sensor [V]
V_s	impingement surface velocity [$m s^{-1}$]
w	nozzle width [mm]
W	width of gold film [m]
x	distance from stagnation point [m].

Greek symbols

α	heat transfer coefficient [$W m^{-2} °C^{-1}$]
α_s	thermal coefficient of resistance [K^{-1}]
δ	thin-film resistivity [Ω m]
ρ	density [$kg m^{-3}$]
ω	circular frequency in equation (9) [s^{-1}]
λ	thermal conductivity [$W m^{-1} °C^{-1}$]
τ_0	cycle time for one rotation of the cylinder [s].

Subscripts

j	at the jet location
o	at the stagnation point
s	sensor.

reasonably well to the substrate and were resistant to slight rubbing, gold was selected as the thin-film material.

The selection of the non-conducting substrate is determined by the requirement that the transient surface temperature response must be the same for the substrate and the surrounding material made of porous stainless steel (316 p.s.s.). As the transient surface temperature response is determined by the $\sqrt{\lambda \rho c_p}$ value of a material [9], it is therefore necessary to match this value between the sensor substrate and the 316 p.s.s.

A ceramic material, Pyroceram 9606 (Corning Glass, Corning, New York), was selected as the sensor substrate because its $\sqrt{\lambda \rho c_p}$ value at 20°C of 2.89 kJ $m^{-2} K^{-1} s^{-1/2}$ calculated from literature [10] was considered close enough to 2.78 kJ $m^2 K^{-1} s^{-1/2}$ obtained for the p.s.s. Another reason for the selection of Pyroceram 9606 is that its thermal physical properties are accurately known and it is recommended [10] as a reference material. The thermal conductivity of the surrounding material, necessary for the determination of $\sqrt{\lambda \rho c_p}$, was measured using the transient method developed by Ioffe and Ioffe [11]. More details on this method are given in refs. [3] and [12].

CONSTRUCTION OF THE HEAT FLUX SENSOR

The thin-film heat flux sensor is shown in Fig. 1. At the Research Laboratory of Corning Glass, the Pyroceram 9606 substrate was machined to have a wide base, thus preventing possible ejection at high rotational speeds of the cylinder used for heat transfer studies.

After fine polishing the Pyroceram substrate with a 0.3-micron Al_2O_3 suspension, a gold film was

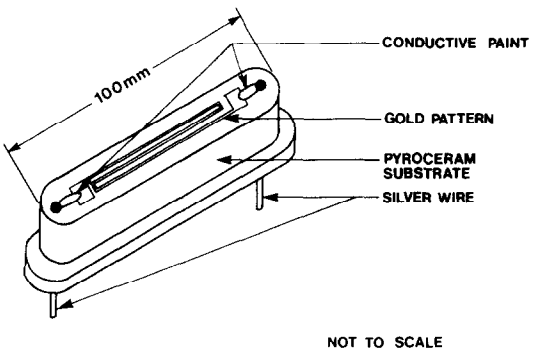

FIG. 1. The heat flux sensor.

deposited uniformly on the substrate by the sputtering technique. As equation (1) indicates, the sensor sensitivity increases with length of the film. This can be achieved by using a zig-zag film pattern. The zig-zag pattern shown in Fig. 1 was obtained by a photofabrication technique consisting of the following steps:

(1) Uniformly coating of the gold film with a positive photoresist.
(2) Exposing the photoresist to uv light via a mask pressed onto the substrate. The mask was made by photographic miniaturization of a large scale model of the zig-zag pattern.
(3) Removing sequentially the exposed photoresist, the underlying gold film and finally the photoresist over the remaining zig-zag gold pattern.

After photofabrication, the sensor was annealed at 300°C for 12 hr. During this process its electrical resistance decreases by about 30%. Finally a protective SiO_2 layer of about 1000 Å thickness is deposited on the gold film by sputtering. For several sensors, the resistivity δ and temperature coefficient of resistance α_s were found to be 6.1×10^{-6} Ω cm and 0.0015 K^{-1} at room temperature regardless of the gold film thickness, which varied from 1300 to 2700 Å. These physical property values are respectively 2.6 times and 1/2.6 times the 'bulk' property values of δ and α_s. The particular sensor used to obtain the local heat transfer results in the present study consisted of three gold strips 0.25×70 mm, each separated by 0.20 mm as shown in Fig. 1. The film thickness of 0.27 μm was calculated using the relationship between the sputtering frequency and gold film thickness on glass as measured by optical interferometry, and by assuming no influence of the substate. A low contact resistance silver paint (Conductive Silver 200 from Degussa) was used to achieve electrical contact between the gold pad at the end of the zig-zag pattern and the 1.3-mm-thick silver lead wires which were glued with epoxy to the Pyroceram substrate. Three thermocouples were glued to the back of the sensor with a high thermal conductivity epoxy adhesive. The junctions were located at the center and at 30 mm from the center and are used for monitoring possible thermal gradients in the largest dimension of the sensor.

SENSITIVITY OF THE HEAT FLUX SENSOR SYSTEM

The sensor was calibrated in a waterproof plastic bag in a thermostat bath and in place in the experimental set-up. The results are shown in Fig. 2. The difference between the calibrations in place and in the thermostat bath is about 0.5 Ω, caused by the lead wires and a small scratch in one of the gold legs, made accidentally during the positioning of the sensor in the cylinder. The upper curve in Fig. 2 is well described by

$$R_s = 174.08 + 0.2742\ T_s + 3.4 \times 10^{-5}\ T_s^2. \quad (2)$$

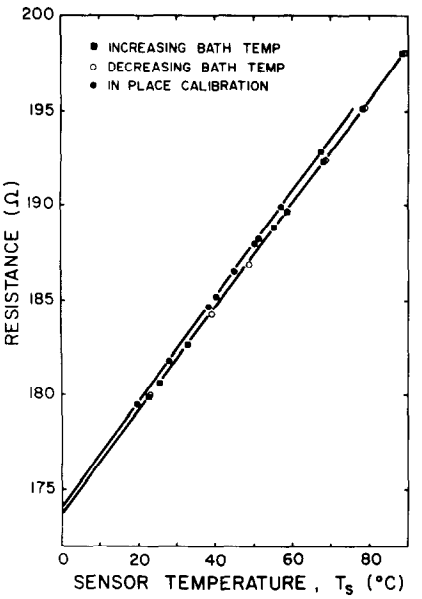

FIG. 2. Calibration curve of heat flux sensor.

The average fluctuating component of the sensor resistance is measured with a four-decade Wheatstone bridge in the circuit shown below. In operation the

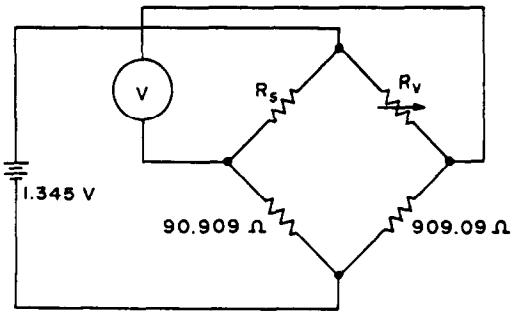

bridge is balanced by setting the variable resistance R_v at 10 times the average of the sensor resistance R_s.

The sensitivity of the heat flux sensor system expressed in V °C^{-1} is

$$S_b = \frac{dv}{dT_s} = \frac{dv}{dR_s}\frac{dR_s}{dT_s}$$

$$= \frac{1.345 \times 909.09(0.2742 + 6.8 \times 10^{-5} T_s)}{(R_s + 90.909)(909.09 + R_v)}. \quad (3)$$

Typically, a variation in bridge voltage output of 1 μV corresponds roughly to a change in sensor temperature of 0.002°C. As a result the electrical noise should be held to the order of a few μV. This was achieved by the following measures:

—Selection of low noise slipring assembly and amplifiers.
—Use of mercury battery instead of regulated DC power supply as the power source for the sensor circuit.

—Grounding all instruments and experimental set-up to the same ground.
—Proper orientation of the instruments.
—Use of shielded wires, with shield connected to a common ground.
—Use of low pass filter with 48 db/oct attenuation slope.
Use of DC carbon piles for power supply and control of heating lamps.

The sensitivity of the sensor system can be increased, by increasing the bridge voltage, as long as self-heating of the sensor is small compared to the heat flux to be measured. The self-heating heat flux q_s resulting from the voltage drop across the thin film is

$$q_s = v_s^2/(LWR_s). \quad (4)$$

For the sensor described here, with an imposed voltage of 0.91 ± 0.005 V, a sensor resistance of about 190 Ω, a film length of 0.21 m and a film width of 0.25 mm, $q_s \cong 83$ W m^{-2}. This value is two orders of magnitude smaller than the typical stagnation heat flux under the impinging jets studied. In fact, self-heating of the sensor leads to a much smaller error than indicated above, because more than 90% of the heat generated in the gold film is removed by conduction through the Pyroceram sensor and less than 10% by convection to the impingement flux [14]. Also the effective surface area for convective heat transfer is larger than the gold film surface due to conduction in the Pyroceram substrate [14]. Thus the self-heating flux effect contributes negligible error in the present test case.

DATA ACQUISITION AND PROCESSING

The bridge voltage is amplified and filtered of high frequency noise before being digitized by a high speed analog-to-digital converter (ADC) and subsequently stored on a disk of a GEPAC 4020 computer. The digitized sensor surface temperatures are calculated from the variable resistor, R_v, and the stored bridge voltages.

A solution of the unsteady one-dimensional heat conduction equation for a semi-infinite solid with a fluctuating surface temperature as boundary condition is available [13], but the numerical evaluation of the integral in the expression for the heat flux at the surface is more complicated and not as fast as the calculation of the heat flux from the numerical solution of the temperature distribution in the semi-infinite solid [8]. The temperature distribution in the solid is calculated by dividing the sensor substrate in n layers of thickness h and using the successive substitution formula [8]

$$T_{r,t} = \tfrac{1}{2}(T_{r-1,t-1} + T_{r+1,t-1}) \quad (5)$$

with $r = 1, 2, 3, \ldots, n-1$ and $r = 0$ referring to the sensor surface. The thickness h is determined by the time between consecutive digitized surface temperature measurements, Δt, as

$$h = \sqrt{2a_s \Delta t}. \quad (6)$$

The heat flux at the surface is calculated by

$$q_{0,t-2/3} = \frac{\lambda}{h}(T_{0,t} - T_{1,t-1}) \quad (7)$$

for $t = 1, 2, 3, \ldots, N$.

The boundary conditions are given by the measured surface temperature $T_{0,t}$ and the semi-infinite boundary condition $T_{n,t} = T_{n-1,t}$. As the initial condition $T_{r,0}$ is set equal to the average surface temperature, the influence of the estimated uniform temperature $T_{r,0}$ is completely eliminated after two complete revolutions of the porous cylinder. The number of finite difference layers is given by $2.0\sqrt{\tau_0/\Delta t}$. This definition leads to an error of 1% in the amplitude of a sinusoidal surface temperature variation of frequency τ_0^{-1} in the numerical scheme [9]. The physical thickness of the sensor of 6.35 mm requires the rotational speed of the cylinder to be larger than 0.36 rev s^{-1} or $\tau_0 \leqslant 2.78$ s.

The fractional error in heat flux amplitude and phase shift for a sinusoidal heat flux variation when using equations (5) and (7), instead of the exact solution of the unsteady heat condution equation are respectively [3, 8]

$$1 - \frac{\sqrt{\sin(2\pi\Delta t/\Delta\tau_m)}}{\sqrt{2\pi\Delta t/\Delta\tau_m}}$$

and $\frac{1}{3}\pi\Delta t/\Delta\tau_m$ radians, $\Delta\tau_m$ being the time for a complete cycle at the highest heat flux frequency.

EXPERIMENTAL SET-UP

As in the "Papridryer", the central component of the experimental set-up is a rotating cylindrical impingement surface. In order that this facility would be operated with throughflow at the impingement surface, the cylinder was constructed of porous stainless steel and has a diameter of 482 mm. Overall steady-state operation is achieved through the use of two slot jets, one hot and one cold, impinging on the cylinder from 180° opposed positions. The flow field of the heating jet and cooling jet is separated by two skimmer plates located midway between the nozzles and very close to the surface of the cylinder, as shown in Fig. 3. The confinement surface was concentric with the cylinder. The spent air exhausts through exit ports located at the confinement surface at positions 90° on either side of the respective inlet nozzle.

The sensor was mounted flush with the cylinder surface, the long dimension of the sensor being parallel to the cylinder axis, and fastened by epoxy as depicted in Fig. 4. The size of the exposed sensor surface is 3.2×100 mm. Thus the sensor width (3.2 mm) is smaller than the widths of the nozzles used (6.2 and 14.1 mm), so that the heat flux measured approaches point value measurements. As the sensor is half the length of the 203-mm-long nozzles and is mounted centrally in the axial direction, the end effect region near the sidewalls is

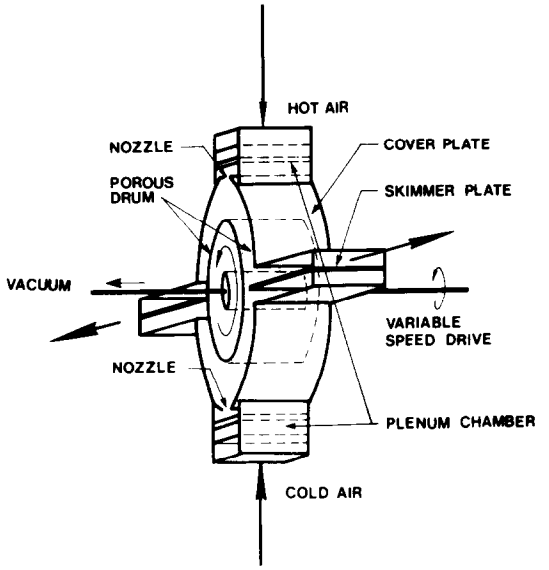

FIG. 3. Schematic view of cylindrical confined impingement apparatus.

avoided. A 50 μm polyimide adhesive tape was used to cover the small gap between sensor and cylinder to avoid flow separation at the edges.

In order to identify the circumferential location of the sensor during rotation, the cylinder was fitted with a lever which activates a microswitch. A square wave voltage signal produced by the microswitch circuit is transmitted to the other channel of the ADC and stored on a disk simultaneously with the signal from the sensor, thus identifying the position of the digitized sensor signal relative to the stationary microswitch.

After calculation of local heat flux for many rotations, local heat transfer coefficients were evaluated as

$$\alpha = q/(T_j - T_s) \tag{8}$$

with T_j being the hot or cold jet temperature at the nozzle exit depending on the position of the sensor. To obtain the mean value of local heat transfer coefficient, the calculated heat transfer coefficient at each circumferential position is averaged generally over 50 rotations, a number which will be shown later to be sufficient. Finally the mean local Nusselt numbers were calculated using the physical properties and dimension at the corresponding nozzle. The plotting of circumferential Nusselt number distributions was done for each jet, with the omission of the first and last 15° of each 180° half-cylinder impingement surface, as conditions in these sections are affected by proximity to the sputter plates and exit ducts.

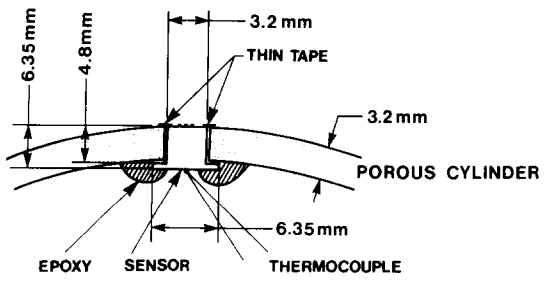

FIG. 4. The heat flux sensor in place.

USE AND VALIDATION OF THE HEAT FLUX MEASUREMENT

Impingement heat transfer represents a particular challenging test of a technique for obtaining local heat transfer data because not only is the bell-shaped distribution a difficult one to obtain for a moving surface but, for a significant range of Reynolds number and spacing from the impingement surface, a pair of large secondary peaks appear on either side of the stagnation peak, so that the complete profiles comprise three maxima and two minima. The treatment of these physical phenomena is the subject of further publications.

Heat transfer data are obtained simultaneously for the upper (heating) and the lower (cooling) jet, respectively, of nozzle widths w, 6.2 and 14.1 mm. The range of the variables spacing, H/w, temperature, driving force $T_j - T_s$ (°C), Reynolds number, Re_j, and impingement surface motion, V_s, are given in Table 1.

(a) Isothermal impingement surface condition

Theoretical and experimental confirmation that the cylinder is essentially isothermal is obtained when, as a first approximation, the cylinder (or heat flux sensor) is considered to be subjected to a sinusoidal heat flux $q = q_0 \sin \omega t$. The amplitude of the surface temperature fluctuation, $|T_s|$, of the cylinder is given by [3, 8]

$$|T_s| = \tfrac{1}{2}\pi \overline{Nu_j} \lambda_j |(T_j - T_s)| / (w\sqrt{\omega \lambda \rho c_p}) \tag{9}$$

with $\overline{Nu_j}$ being the average Nusselt number on the heating or cooling side of the apparatus and λ_j the thermal conductivity of air at the jet temperature. The calculated amplitude $|T_s|$ and half of the measured gold film sensor temperature fluctuation during a complete revolution, $\frac{1}{2}\Delta T_{sm}$, are compared in Table 2 for four limiting cases for the cooling jet, i.e. for high and low impingement surface velocity, V_s, and high and low Re_j. The result of $\frac{1}{2}\Delta T_{sm} \approx 1.2|T_s|$ is not unexpected since the sharp increase in heat transfer directly under the jets leads to a slightly larger amplitude than that calculated

Table 1. Range of parameters for experiments

w (mm)	14.1	6.2
H/w	2.6	6.0
$T_j - T_s$ (°C)	−10.8 – −38.6	21.3–48.7
Re_j	9700–91800	5200–20300
U_j (m s^{-1})	12–115	20–70
V_s (m s^{-1})	0.6–13.0	0.6–13.0

Table 2. Impingement surface temperature fluctuation

Run	V_s (m s^{-1})	ω (rad s^{-1})	Re_j	T_j (°C)	$T_s - T_j$ (°C)	$\overline{Nu_j}$	$\lvert T_s \rvert$ (°C)	$\frac{1}{2}\Delta T_{sm}$ (°C)
148	0.60	2.51	9700	34.8	32.2	~19	0.41	0.49
163	1.03	4.27	91500	39.3	19.8	~95	0.98	1.12
152	13.0	53.8	11100	36.6	35.6	~16	0.082	0.11
219	11.9	49.3	89000	30.0	21.8	~83	0.26	0.32

from a smooth sinusoidal fluctuation. From these results it is also clear that the surface temperature fluctuation on the cooling jet side for the extreme case (run 163, high Re_j and low V_s) is still only 6% of the temperature driving force, $T_j - T_s$. Because $T_s - T_j$ on the heating side is generally about 1.5–2 times larger, the isothermal condition applies even more closely on the heating jet side.

(b) Number of rotations averaged for a profile

The fluctuations in heat flux at a fixed circumferential position are mainly due to the turbulent character of the flow and, to some extent, to the slower oscillations in the hot jet temperature (oscillations of ± 1°C with a frequency of 0.1–0.05 s^{-1}). The temporal fluctuations can be eliminated by averaging the local heat flux at a specific location over a number of rotations. With increasing number of rotations the Nu distribution becomes smoother while maintaining exactly the same basic shape and same position as shown for 1 and 50 rotations in Figs. 5a and 5b, respectively (results for 1, 5, 25 and 50 rotations are available in ref. [3]). These figures show profiles of local Nusselt number as a function of lateral distance, the latter shown both as the non-dimensional position x/w and the angular circumferential position. The position $x/w = 0$ is at the stagnation point for slow rotation (< 1 rev s^{-1}) and is at the nozzle centerline for all cases. From the small difference between the distributions obtained for averaging over 25 and 50 rotations it was decided that averaging over 50 rotations was adequate for smoothing and reproducability and should be used for all the experiments.

(c) Filtering of noise from the heat flux sensor signal

The low-pass filter frequency was varied to establish experimentally the minimum frequency to obtain an undistorted low-noise heat flux signal. The results for a rotational speed of about 25 rev min^{-1} and an ADC sampling frequency of 200 measurements s^{-1} are shown in Fig. 6 for the bottom jet. The heat flux and angular position at the stagnation point as a function of the filter frequency are given in Table 3. The results with a filter frequency of 300 Hz do not differ significantly from the results with 1000 Hz. By decreasing the filter frequency below 300 Hz the heat flux distribution is displaced appreciably in the scanning direction. Filtering at 30 Hz introduces an error of about 5% in the

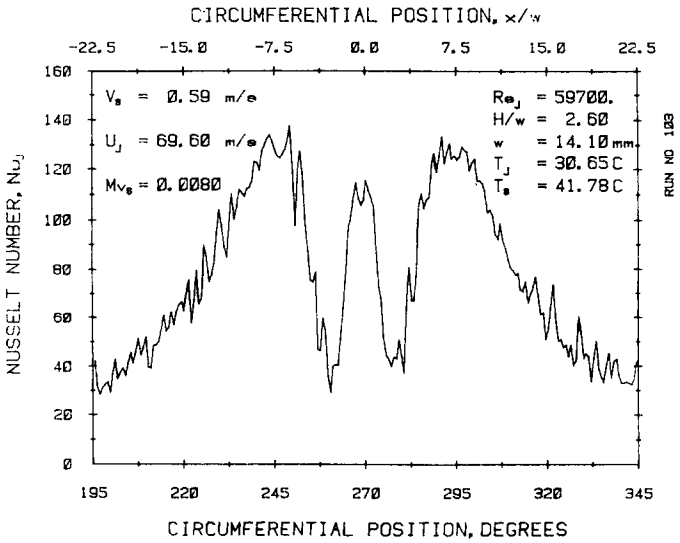

FIG. 5a. Effect of number of rotations for averaging the heat transfer distribution: $N_R = 1$.

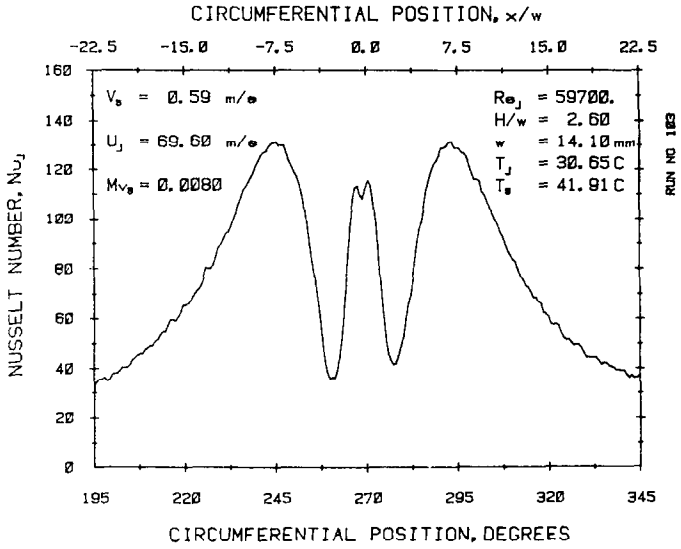

FIG. 5b. Effect of number of rotations for averaging the heat transfer distribution: $N_R = 50$.

heat flux amplitude. It can be seen from Fig. 6 that the small dip in the central heat transfer peak (frequency ~ 60 Hz) of the bottom jet disappears as expected with a filter frequency of 30 Hz. Since the number of measurements per rotation was fixed at about 500 for all rotational speeds, these results demonstrate that the filter frequency should be larger than the ADC sampling frequency to obtain an essentially undistorted and undisplaced heat flux distribution, while removing most of the high frequency noise. The number of 500 measurements per rotation was established experimentally as being the optimum value whereby full resolution of the heat transfer profile is obtained without excessive noise yet within a modest computation time.

(d) Independence from T *of the* Nu *data produced by this technique*

The temperature driving force was raised for the cooling jet from about 10 to 40°C and for the heating jet from about 20 to 50°C. The results of the variable temperature difference, $T_j - T_s$, on the heat transfer for the heating jet at $Re_j = 13800 \pm 100$ are compared in Table 4 at three locations: at the stagnation point, Nu_{oj}; at the off-stagnation maximum, Nu_{jm}; and over the averaging distance $-25.5 \leqslant x/w \leqslant 25.5$, $\overline{Nu_j}$. These results, as well as those for the cooling jet, show that profiles of Nusselt number defined at the jet temperature, T_j, are independent of the size and direction of the temperature driving force. The independence of Nu_j from the temperature driving

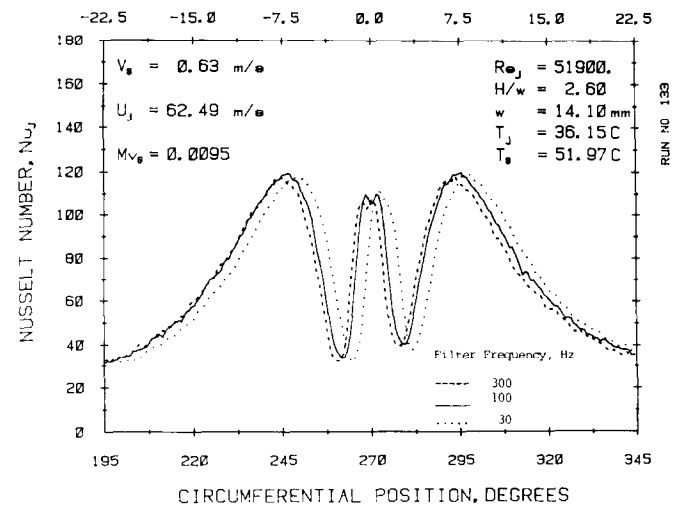

FIG. 6. Effect of frequency of low-pass filter.

Table 3. Effect of filter frequency on magnitude and position of stagnation point heat flux

Run No.	Filter frequency (Hz)	Nu_o	Position (degrees)
130	1000	102.3	270.4
132	300	100.5	271.0
131	100	101.1	271.7
133	30	107.7	274.0

force provided further confirmation that this heat flux sensor and associated procedures produces reliable data.

(e) Validation of the technique based on previous results for stationary heat transfer surfaces

Further evidence of the accuracy of results from the thin-film sensor in the rotating impingement cylinder equipment is obtained by comparing the present heating jet heat transfer profiles with the generally accepted results of Gardon and Akfirat [15] and Cadek [16]. Cadek used the same thin-disk heat flux sensor as Gardon and Akfirat, known as the Gardon foil, after the first author of ref. [15] who developed this type of sensor. The diameter of the Gardon foil is 0.9 mm, i.e. 0.28w or 0.14w, respectively, in Cadek's and Gardon's experimental set-up, compared to 1.15 mm for the effective gold film width or 0.19w and 0.08w for the present heating and cooling jet, respectively. Accurate calibration of the Gardon foil is quite difficult as the maximum output is less than 10 μV at the highest impingement heat flux rates. Because of the low sensitivity of the Gardon foil of 0.91 μV (kW m^{-2})$^{-1}$, Cadek [16] only used the heat flux meter for measurement of heat transfer rates relative to the stagnation heat transfer. Gardon [15] also used the foil for relative measurements and admits that the sensor calibration in a previous study was 40% too high.

As the present profiles obtained at low impingement surface speed are essentially symmetric, both sides of the profiles of the present study for $Re_j = 11000$ are, for convenience, used in Fig. 7 to display measurements of the two reference studies. The results are in excellent agreement over the critical impingement region. In fact, examination of Fig. 7 indicates that the transition point minimum and secondary maximum are defined more precisely by the experimental techniques developed for the present study. Another example of excellent agreement with the heat transfer data of Cadek [16] in the impingement and early wall jet region as well as high resolution of the present experimental technique is given in Fig. 8 for the cooling jet at $H/w = 2.6$ at $Re_j = 52100$.

(f) Use of the technique with a moving heat transfer surface

The fast response time of the sensor becomes crucial for the determination of local flux with a fast moving heat transfer surface. Results for this case are displayed in Fig. 9. These results show the local Nusselt number profiles obtained for impingement surface motion, V_s, expressed in the appropriate non-dimensional parameter, $M_{V_s} = V_s\rho_s/U_j\rho_j$ varying between $V_s = 0.91$ m s^{-1} ($M_{V_s} = 0.03$) and $V_s = 12.74$ m s^{-1} ($M_{V_s} = 0.4147$). At the highest rotational velocity, the time between two consecutive digitized surface temperature measurements taken by the sensor is 0.25 ms, giving a total measurement time of about 6 s for 50 cylinder revolutions to define the complete local heat transfer distribution for the cooling as well as for the heating impinging jet. As no one has previously succeeded in developing an experimental technique for measuring local heat transfer for jets impinging on a surface which is moving, there are no published heat transfer profiles to compare with. Even for the case of average rather than local heat transfer for a moving surface under impinging jets, there are only two studies available, those of Fechner [17] and Subba Raju and Schlünder [18]. The average results of Fechner agree with those of the present study, while analysis indicates that the results of the latter study are in error.

All the validation tests described above are an indirect verification of the accuracy of the present heat flux sensor system. An absolute verification of the sensitivity of the sensor, for example by exposing the sensor to a well defined non-contact heat flux for a short

Table 4. Influence of $(T_j - T_s)$ on heat transfer for the heating jet

Run No.	Re_j	T_j (°C)	$(T_j - T_s)$ (°C)	Δp (mm H_2O)	Nu_{oj}	Nu_{jm}	$\overline{Nu_j}$*
185	13700	99.1	41.8	12.6	63.4	35.7	27.2
186	13800	98.7	38.2	12.6	63.7	36.5	27.5
187	13700	99.4	33.8	12.6	62.0	35.3	26.5
218	13900	101.2	48.7	13.1	65.3	37.0	28.0
222	13900	80.0	33.2	10.7	64.6	35.8	27.6
224	13900	80.3	31.4	10.7	63.7	36.1	27.2
225	13900	71.4	22.6	9.8	63.3	35.5	27.2

* Averaged over $-25.5 \leqslant x/w \leqslant 25.5$, or $-4.25 \leqslant x/H \leqslant 4.25$.

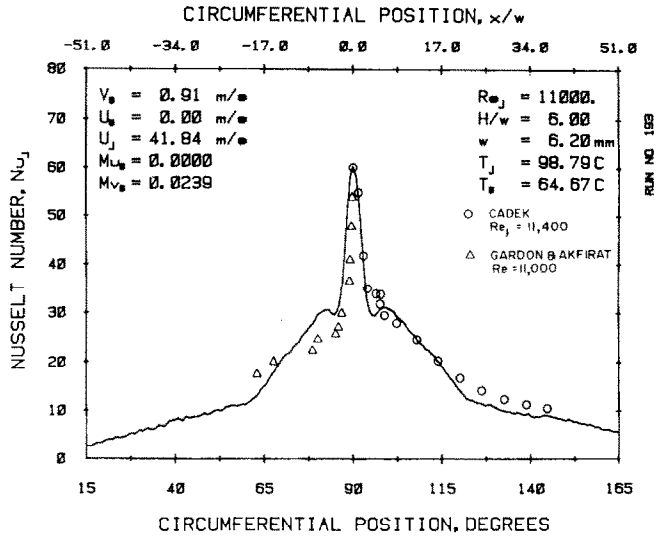

FIG. 7. Lateral profiles of Nu_j at $H/w = 6$: comparison of results.

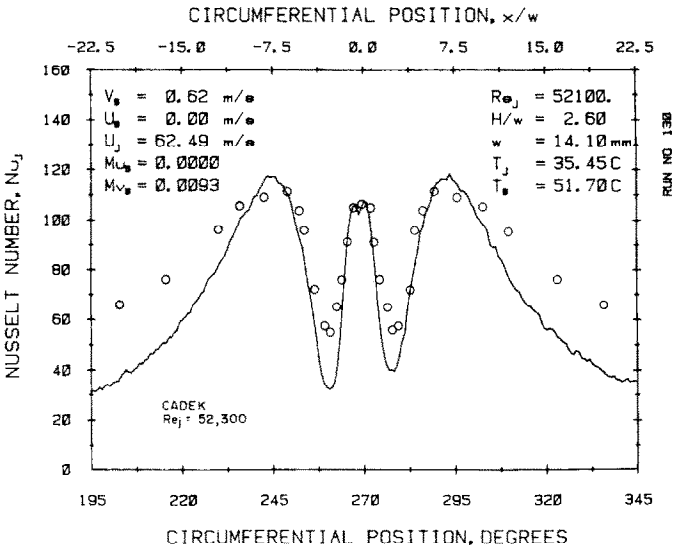

FIG. 8. Lateral profiles of Nu_j at $H/w = 2.6$: comparison of results.

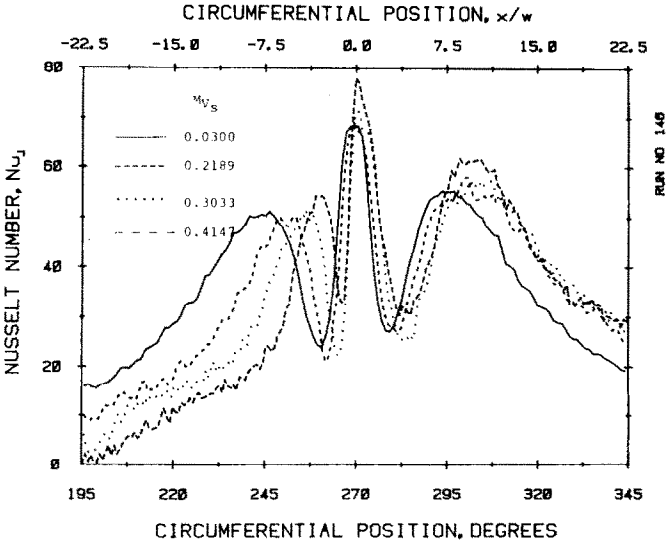

FIG. 9. Effect of M_V on lateral profile of heat transfer at $Re_j = 23000$ and $H/w = 2.6$.

period of time, was not undertaken because of the inaccuracy of these tests resulting from the unknown sensor surface emissivity (gold and Pyroceram) and because of the difficulty of generating an accurately known and well-defined heat flux.

CONCLUDING REMARKS

A high sensitivity, fast response thin-film flux sensor was developed which has made it possible to measure local heat flux at a moving surface subjected to a complex, fluctuating heat flux. This sensor and the associated measurement system was validated for one such flow, that of a jet impinging on a moving surface, but is generally applicable for problems involving rapidly fluctuating heat fluxes or short measuring times. The uniqueness of the present measurement system is illustrated by the fact that this is the first and only study to date whereby local impingement heat transfer profiles have been measured for the industrially important case of fast moving continuous surfaces.

Acknowledgement—The help of Dr M. C. Jain of Precision Photomask, St. Hubert, Quebec, Canada, is gratefully acknowledged.

REFERENCES

1. B. W. Burgess, S. M. Chapman and W. Seto, The Papridryer Process. Part I, The basic concepts and laboratory results, *Pulp Pap. Can.* **73**, 314–322 (1972).
2. B. W. Burgess, W. Seto, E. Koller and I. T. Pye, The Papridryer Process. Part II, Mill trials, *Pulp Pap. Can.* **73**, 323–331 (1972).
3. A. R. P. van Heiningen, Heat transfer under an impinging slot jet. Ph.D. thesis, Dept. of Chem. Eng., McGill University, Montreal (1982).
4. P. H. Rose, Development of the calorimeter heat transfer gauge for use in shock tubes, AVCO Research Report 17 (February 1958).
5. W. D. Baines and J. F. Keffer, Shear stress and heat transfer at a stagnation point, *Int. J. Heat Mass Transfer* **19**, 21–26 (1976).
6. K. R. Scheuter and G. A. Dosdogru, Die Messung der örtlichen Wärmeübergangszahl mittels eines geheizten Bandes, *Schweizer Arch. angew. Wiss. Tech.* **10**, 36 (1970).
7. A. R. P. van Heiningen, A. S. Mujumdar and W. J. M. Douglas, On the use of hot and cold-film sensors for skin friction and heat transfer measurements in impingement flows, *Letters Heat Mass Transfer* **3**, 523–528 (1976).
8. D. J. Baines, A comparative theoretical evaluation of five commonly used types of unsteady heat flux sensor, Report HSA 27, Australian Defence Scientific Service, Weapons Reserach Establishment (1970).
9. E. R. G. Eckert and R. M. Drake, Jr., *Heat and Mass Transfer*, 2nd edn, pp. 76–109. McGraw-Hill, New York (1959).
10. Y. S. Touloukian, *Thermophysical Properties of Matter*. IFI/Plenum, New York (1970).
11. A. V. Ioffe and A. F. Ioffe, Measurements of thermal conductivity of semiconductors in the vicinity of room temperature, *Soviet Physics—Technical Physics* **3**, 2163–2168 (1958).
12. O. Biceroglu, A. S. Mujumdar, A. R. P. van Heiningen and W. J. M. Douglas, Thermal conductivity of sintered metal powders at room temperature, *Letters Heat Mass Transfer* **3**, 183–192 (1976).
13. H. S. Carslaw and J. C. Jaeger, *Conduction of Heat in Solids*. Oxford University Press (1959).
14. R. I. Tanner, Theory of a thermal flux meter in a shear flow, *J. appl. Mech.* **34**, 801–805 (1967).
15. R. Gardon and J. C. Akfirat, Heat transfer characteristics of impinging two-dimensional air jets, *J. Heat Transfer* **88**, 101–108 (1966).
16. F. F. Cadek, A fundamental investigation of jet impingement heat transfer. Ph.D. thesis, University of Cincinnati (1968).
17. G. Fechner, Wärmeübertragung bei senkrecht auftreffendem Strahl an der Platte und am Rohr. Dissertation, T.U. München (1971).
18. K. Subba Raju and E. U. Schlünder, Heat transfer between an impinging jet and a continuously moving flat surface, *Wärme-u. Stoffübertr.* **10**, 131–136 (1977).

UN FLUXMETRE THERMIQUE A HAUTE SENSIBILITE ET A REPONSE RAPIDE

Résumé—Un fluxmètre thermique à haute sensibilité et réponse rapide est réalisé pour des mesures de flux sur une surface mobile et soumise à des flux thermiques rapidement fluctuants. La sonde est une résistance à film mince en or sur un substrat non conducteur. Montée sans surépaisseur avec la surface mobile, la sonde mesure la température instantanée de la surface avec une résolution proche de 0,002°C à des vitesses d'échantillonnage de 5000 s^{-1}. Le flux thermique local est obtenu à travers la résolution de l'équation de conduction de la chaleur. Des profils de transfert thermique sont déterminés avec cette technique dans le cas de jet plans frappant des surfaces mobiles à des vitesses qui atteignent 12 m s^{-1}.

EIN HOCHEMPFINDLICHES, SCHNELL ANSPRECHENDES MESSGERÄT FÜR DIE WÄRMESTROMDICHTE

Zusammenfassung—Ein hochempfindliches, schnell ansprechendes Meßgerät für die Wärmestromdichte an bewegten Oberflächen, die schnell schwankenden Wärmeströmen unterworfen sind, wurde entwickelt. Das Meßgerät ist ein Dünnfilm-Widerstandsthermometer aus Gold mit nichtleitendem Trägermaterial. Das Meßgerät registriert die momentane Oberflächentemperatur mit einer Auflösung von 0,002 K bei maximal 5000 Messungen pro Sekunde. Die lokale Wärmestromdichte wird durch Lösung der instationären Wärmeleitungsgleichung ermittelt. Mit dieser Technik ergaben sich Wärmetransportprofile für den Fall eines ebenen Strahls, welcher auf Oberflächen auftrifft, die sich mit Geschwindigkeiten bis 12 m s^{-1} bewegen.

ВЫСОКОЧУВСТВИТЕЛЬНЫЙ БЫСТРОДЕЙСТВУЮЩИЙ ДАТЧИК ТЕПЛОВОГО ПОТОКА

Аннотация—Для измерения теплового потока у движущейся поверхности, подверженной действию быстро флуктуирующего теплового потока, создан высокочувствительный быстросрабатывающий датчик. Датчик представляет собой термометр сопротивления из тонкой золотой пленки на непроводящей подложке. Установленный заподлицо с движущейся поверхностью датчик измеряет мгновенную температуру поверхности с разрешающей способностью ~0,002°С при скоростях ее изменения, соответствующих верхней частоте спектра до 5000 Гц. Локальный тепловой поток определяют путем решения уравнения нестационарной теплопроводности. Профили тепловых потоков строились при помощи данной методики для случая плоских струй, натекающих на поверхности, движущиеся со скоростями до 12 м/с.